Calcif Tissue Int (1992) 51:363–369

Calcified Tissue International

Nacre Initiates Biomineralization by Human Osteoblasts Maintained *In Vitro*

Caroline Silve,[1] Evelyne Lopez,[2] Bernadette Vidal,[2] David C. Smith,[3] Serge Camprasse,[4] Georges Camprasse,[4] and Gérard Couly[5]

[1]CNRS URA 583 and [2]Service de Stomatologie, Hôpital Necker Enfants Malades, 149 rue de Sevres, 75015 Paris, France; [3]CNRS URA 90, Laboratoire de Physiologie Générale et Comparée and [4]Laboratoire de Minéralogie, Muséum National d'Histoire Naturelle, Paris, France; and [5]Cabinet Dentaire, Chelles, France

Received November 22, 1991, and in revised form February 19, 1992

Summary. When nacreous shell produced by the marine oyster *Pinctada maxima,* used as a biomaterial in oral surgery, is implanted in human bone, new bone formation occurs, resulting in a tight welding of the bone to the nacre [16]. These findings are consistent with the possibility that nacre adjacent to bone can locally stimulate osteogenic activity. To test this hypothesis, we have evaluated the effect of the simultaneous presence of bone and nacre on human osteoblasts *in vitro*. Nacre chips (1 mm^3) were placed at ≈1 mm distance from a similarly sized bone chip on a layer of first passage human osteoblasts. None of the chemical inducers generally required to obtain bone mineralization *in vitro* (in particular, β-glycerophosphate) was added to the cultures. Mineralized sections of the cultures were evaluated by light and electron microscopy, contact microradiography, and Laser Raman Spectroscopy. The results demonstrated that nacre has strong osteogenic effects on human osteoblasts when placed in proximity to bone *in vitro*. New bone formation occurred by both appositional growth on the existing bone and by the formation of mineralized nodules within the matrix adjacent to the bone explant. Electron microscopic evaluation of these sites demonstrated findings typical of those described in the course of bone formation *in vivo,* and no evidence of toxicity was observed. In addition, under the conditions of culture used, nacre can also promote the formation by osteoblasts of a structure with characteristics similar to nacre (e.g., lamellar organic matrix mineralized with aragonite, as demonstrated by Laser Raman Spectroscopy). Given the unusual capacity of nacre in the presence of human osteoblasts *in vitro* to induce different types of mineralization, this model should provide insights into the specific interactions between matrix proteins and minerals that control the type of mineral produced in the course of biomineralization.

The formation of bone by osteoblasts is the result of a series of events that include the secretion of matrix proteins, the specific organization of the matrix in a fashion that promotes crystal nucleation, and the secretion of ions necessary for mineral growth [1, 2]. Better understanding of these events is essential to our understanding of bone growth, and would have important clinical implications in situations where the ability to specifically stimulate new bone formation would be beneficial.

Currently, the factors controlling these steps *in vivo* are poorly understood. The availability of an *in vitro* model of normal bone formation would be of considerable use in studying these questions. When osteoblasts are maintained *in vitro,* however, bone formation does not occur spontaneously. As a consequence, virtually all studies of *in vitro* mineralization have used chemical inducers, especially β-glycerophosphate, to stimulate bone mineralization. β-glycerophosphate clearly modulates alkaline phosphatase activity and mineral deposition by cultured osteoblasts [3–13]. The physiological relevance of the initiation of mineralization by β-glycerophosphate, however, is not clear. Mineralization in the presence of β-glycerophosphate but in the absence of osteoblasts has been demonstrated [14], and cellular toxicity has been observed in the presence of β-glycerophosphate [14, 15]. In addition, when β-glycerophosphate is added to bone explants, the sites at which mineralization occur cannot be controlled and bone formation occurs at ectopic sites in the periosteum, not by appositional growth on existing bony surfaces [15]. Thus, the identification of substances that induce controlled appositional growth of bone remains a worthwhile goal. In particular, materials that could be used as implants and that have intrinsic osteogenic properties in the local milieu would be very useful.

Campraste et al. [16] have previously shown that when nacreous shell produced by the marine oyster *Pinctada maxima,* used as a biomaterial in oral surgery, is implanted in human bone, new bone formation occurs, resulting in a tight welding of the bone to the nacre. These findings are consistent with the possibility that nacre adjacent to bone can locally stimulate osteogenic activity. To test this hypothesis, we have evaluated the effect of the simultaneous presence of bone and nacre on human osteoblasts *in vitro*. The results demonstrate that biomineralization is strongly stimulated at sites where nacre is in close proximity to bone. Interestingly, the biominerals deposited adjacent to the preexisting bone and nacre had different morphologic, birefringent, and spectrometric features, which resembled those of bone and nacre, respectively.

Materials and Methods

Primary Osteoblast Cultures

Human osteoblasts were grown from biopsies of alveolar maxillary

Offprint requests to: C. Silve

bone obtained from seven children (aged 1–5 years, mean 2.1 years) undergoing necessary surgery as previously described [17] with slight modifications. Bone biopsies were cut into small chips (1 mm^3), incubated for 5 minutes in a lysing solution (10 mM $KHCO_3$, 156 mM NH_4Cl, in H_2O) to lyse red blood cells, and extensively rinsed with BGJb medium (Eurobio, Les Ulis, France) without calcium, supplemented with 100 U/ml penicillin G, 100 μg/ml streptomycin, and 10% fetal calf serum (FCS). Bone chips were then cultured in the same medium in 10 cm^2 culture dishes (Corning), and cells were allowed to grow from the bone explants. Cultures were maintained at 37°C in 95% air/5% CO_2, and medium was changed every third day until cells reached confluence (approximately 2–3 weeks). Cultures were then trypsinized, filtered through a nylon cloth (35 μm mesh) to remove bone pieces, and cells were replated at a density of 5×10^4 cells/cm^2 in 10 cm^2 culture dishes and cultured in 3 ml of BGJb medium (1.2 mM Ca^{2+}, 2.2 mM PO_4, pH 7.4) supplemented as for primary cultures. All experiments were performed on first passage cells.

The osteoblastic phenotype of the cells used for the experiments described was confirmed by (1) the secretion of bone gla protein (BGP) in the absence and presence of 10^{-9} M $1,25(OH)_2D$ for 3 days (8.1 ± 0.8 and 55.2 ± 4.3 ng/100 μg protein, respectively); (2) alkaline phosphatase activity (9.4 ± 0.8 IU/100 μg protein); (3) production of cAMP in response to 8×10^{-8} M human parathyroid hormone 1-34 (PTH) (1.2 ± 0.1 and 16.2 ± 2.6 pmol cAMP/10 minutes/100 μg protein, respectively without and with PTH); and (4) synthesis of type I collagen, as detected by indirect immunofluorescence using rabbit anti-human type I collagen antiserum (Institut Pasteur, Lyon, France).

Evaluation of the Effect of Nacre on Mineralization

Fragments of nacre produced by *P. maxima* were obtained as previously described [16] and sterilized for 30 minutes at 100°C for the experiments. Fragments of human bone were those previously cultured to obtain bone cells, and were not devitalized. To initiate experiments, 1 mm^3 nacre chips were placed at ≈1 mm distance from a similarly sized bone chip on a layer of first passage human osteoblasts 48 hours after subculture. Bone fragments and osteoblast lines were obtained from the same individual in all cases. Cultures containing bone chips only or neither bone nor nacre chips were prepared in parallel. Culture medium was as described for primary cultures; medium was replaced every 4th day. Neither chemical inducers generally required to obtain bone formation *in vitro* (in particular, β-glycerophosphate) nor ascorbic acid was added to the cultures. Human bone cells were the only cells present, as nacreous shell is acellular [18–20]. Periodically, cultures were photographed using a Leitz Diavert microscope fitted with a Photo Automat MPS 45. After 4–6 weeks of culture, medium was removed and samples were fixed as described below.

Light and Electron Microscopic Evaluation of Cultures

For light microscopic examination, undecalcified samples were fixed in Karnowsky medium, embedded in methylmethacrylate [21], and 100 μm sections were prepared using an Isomet microtome (Buehler, Ill, USA) fitted with a low speed diamond saw. Undecalcified sections were ground by hand to a 15–25 μm thickness, stained with basic fushin or toluidine blue/methylene in veronal buffer, and examined using a Carl Zeiss microscope (Jenal Fluoval, RDA) under transmitted light. Photomicrographs were made using a Zeiss automatic camera.

For electron microscopic examination, cultures were fixed *in situ* in 2% glutaraldehyde in 0.1 M cacodylate buffer (pH 7.4) for 1 hour at 4°C, postfixed in 2% osmium tetroxide in 0.1 M cacodylate buffer for 1 hour at 4°C, and embedded in spurr resin. Regions adjacent to the bone chip were identified by low-power microscopy. Ultrathin sections of these regions were cut using a UM III ultramicrotome (LKB, Bromma, Sweden) fitted with a diamond knife, stained sequentially in uranyl acetate and lead citrate, and examined with a Hitachi HU 12 transmission electron microscope. Observations were also made on sections stained with lead citrate only, as it is known that uranyl acetate can result in partial demineralization of sections [22].

Microradiography

Contact microradiographs of each undecalcified section before grinding (100 μm) were made with a PW 1008 Massiot-Phillips X-ray apparatus using a K_α copper target; exposures were made at 30 kV and 20 mA on Kodak 649-0 film.

Laser Raman Spectroscopy

Specimens for laser Raman spectroscopy were prepared as described above for light microscopy, and analyzed using a Raman microprobe [23–26] (Société Dilor) as follows: objective ×50; green Argon laser excitation at 514.53 nm; laser power 100–200 mW; multichannel detection in the range 131–1201 cm^{-1} with two batteries of 1204 diodes; slit width 100–150 μm; 20 accumulations of 5 seconds; peak position calibration corrected to standard diamond at 1332 cm^{-1}.

Results

Effect of Nacre on Osteoblasts In Vitro

When bone chips were placed in proximity of similarly sized nacre chips on a layer of confluent human osteoblasts, the gap between the adjacent bone and nacre was progressively filled over a 4–6 week period by dense tissues extending from the opposing surfaces of both the bone and nacre in all experiments (n = 7) (Fig. 1). Light microscopic observations confirmed that these tissues were continuous between the opposing surfaces of bone and nacre, and were formed by a matrix containing both fibrous and cellular elements (Fig. 2). Collagen fibers were oriented along an axis extending from the bone explant towards the nacre (Fig. 2a). Foci with histologic features typical of nodules of mineralization were observed within the matrix in the proximity of bone (Fig. 2b, d). Photomicroradiographs confirmed that the newly formed matrix was being mineralized, as indicated by the formation of radiodense material, both at the surfaces of the bone and nacre chips, and within the matrix formed between the two surfaces (Fig. 2c, e).

Two aspects of the matrix formation and subsequent mineralization observed in these experiments should be emphasized. First, the process was localized, in that matrix formation and mineralization extending from the surface of the chips occurred only in the space between the bone and nacre. In contrast, no bone growth was observed on the surface of bone distant from the nacre. The surface of the nacre at a distance from the bone explant was covered by osteoblasts, and some matrix deposition occurred, but did not extend from the surface of the nacre. Second, mineralization occurred only when nacre and osteoblasts were present. When osteoblasts were cultured without bone or nacre explants, nodule formation was not observed and mineralization did not occur. When bone chips were cultured in isolation on human osteoblasts, no evidence of bone growth was seen. Only unmineralized fibrous tissue was formed when two bone chips were cultured next to each other in a similar model (data not shown). No modifications were observed on the surface of nacre cultured in the absence of osteoblasts.

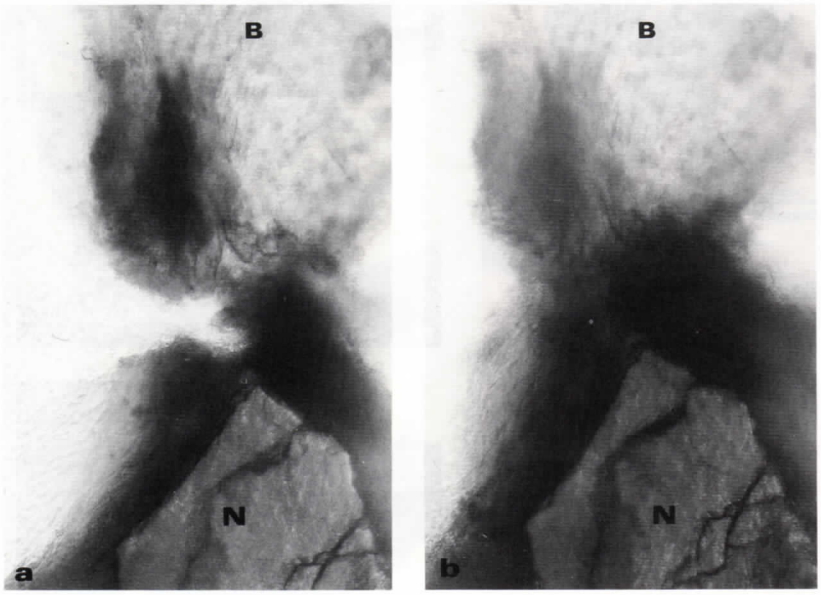

Fig. 1. Phase contrast photomicrographs of bone (B) and nacre (N) explants cultured on a layer of human osteoblasts after (a) 1 and (b) 6 weeks. After 6 weeks, the gap between the two explants is filled by newly formed tissues extending from the opposing surfaces of the bone and nacre (200).

Characterization of Mineralized Tissues Forming Adjacent to Bone and Nacre

Although biomineralization occurred throughout the space between the bone and nacre, as indicated by the formation of radiodense material, the processes occurring proximal to the two surfaces had the following distinctive features.

Mineralization Adjacent to Bone. The newly mineralized tissue which formed adjacent to the bone chip could be readily distinguished from the preformed bone. The newly formed material was woven bone, not lamellar bone as is present in the bone chips, and therefore had a distinctive coarsely fibrous appearance at the light microscopic level (Fig. 2b). In addition, the newly formed bone was more mineralized, and thus appeared more electron dense at the electron microscopic level than the bone explant which was demineralized by the culture (Fig. 3a).

Electron microscopic examination of sites of mineralization occurring at the surface of or proximal to the bone explant revealed findings associated with bone formation *in vivo*. Active osteoblasts with multiple cytoplasmic processes and abundant rough endoplasmic reticulum were present (Fig. 3d), and the extrusion of collagen fibrils and release of matrix vesicles by these cells were observed (Fig. 3d, e). In the proximity of sites of mineralized matrix, coalescent matrix vesicles containing needle-shaped apatite crystals were present (Fig. 3b). The mineralization of collagen fibrils synthesized by the osteoblasts was also apparent (Fig. 3f).

Mineralization Adjacent to Nacre. Newly mineralized tissue formed adjacent to the nacre could also be distinguished from the original nacre fragment. Because the original nacre fragment was more rigid than the newly formed tissue, it could be dislodged, leaving a "mold" of newly mineralized tissue (Fig. 2b, f, and g). Furthermore, in contrast to the original nacre, the newly mineralized tissue forming adjacent to the nacre fragment was stained with basic fushin, due to the presence of abundant mineralizing organic matrix (Fig. 2f, g). The mineralized tissue forming adjacent to the nacre explant differed in several respects from that forming adjacent to the bone fragment. First, the birefringence of the mineralized matrices forming adjacent to bone and nacre were different under polarized light observation (data not shown). Second, in contrast to the coarsely fibrous appearance of mineralized tissue formed adjacent to bone, mineralized material formed adjacent to the nacre was composed of lamellar sheets reminiscent of those present in nacreous shell (Fig. 2c, f, and g). In some sites, "honeycomb" structures, resembling the polygonal prismatic arrangement seen in cross-sections of nacreous material, were observed in direct contact with material more typical of newly mineralized bone matrix (Fig. 3c).

Identification of Newly Formed Mineral by Laser Raman Spectroscopy

Because of the distinctive morphology and birefringence of the newly mineralized material forming in proximity to the nacre fragment, the chemical and structural nature of the crystals present at these sites was evaluated. To do so, laser Raman spectroscopy was performed on 1 μm^3 volumes of tissue present in both mineralized nodules formed between the nacre and bone explants and in newly mineralized tissues forming adjacent to the nacre explant (see Fig. 2f). Strikingly, these spectra demonstrated all of the critical peaks (within ± 3 cm^{-1}) characteristic of orthorhombic $CaCO_3$ (aragonite): 154 (strong), 181 (weak), 207 (strong), 705 (medium), 1087 (very strong) (Fig. 4, spectra c and d). The position of the peaks present in the spectra obtained from the newly mineralized tissue were identical to those obtained from our nacre standard (Fig. 4, spectrum b) and those previously published for aragonite [24, 25]. The spectra obtained from newly mineralized tissues were, however, weaker (greater fluctuations in the baseline), indicating a lower degree of crystallinity of newly formed mineral compared with that of the nacre explant. Spectra also contained an additional peak at 813 cm^{-1}, and smaller massifs around 600, 650, and 1000 cm^{-1}, which correspond to the superimposed spectrum of the methylmetacrylate mounting medium (Fig. 4, spectrum a). No other significant peaks were present, thus proving the aragonite structure of these crys-

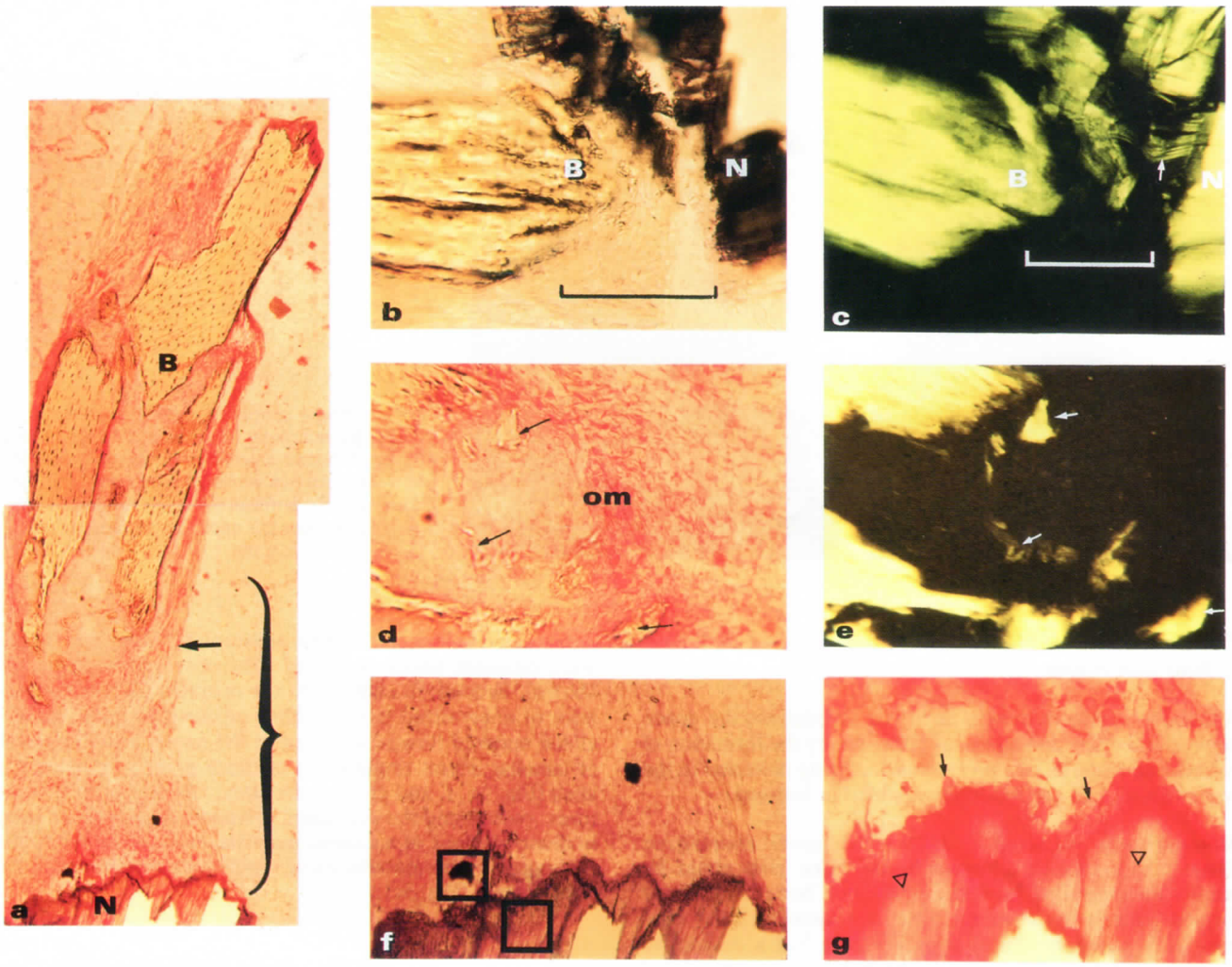

Fig. 2. **(a)** Low power light photomicrograph showing the bone explant (B), the region between the bone and nacre (bracket), and the newly formed mineralized matrix lining the cavity which was occupied by the original nacre explant (N) (40). A dense network of cells and matrix fills the gap between the bone and nacre. Collagen fibers (black arrow) run parallel to an axis extending between the bone and nacre. **(b)** Light photomicrograph of the bone/nacre interface (bracket) demonstrating the intimate contact occurring between the newly formed tissues and the bone (B) and nacre (N) (100). **(c)** Photomicroradiograph of the same region shown in **b,** demonstrating the presence of radiodense mineral in the newly formed tissues. Note the lamellar structure of the tissue formed next to the nacre (white arrow) (100). **(d)** Photomicrograph of the matrix adjacent to the bone explant, showing typical nodules of newly formed bone (small arrows) within the densely basophilic osteoid matrix (om) (100). **(e)** Photomicroradiograph of the same region shown in panel **d,** demonstrating the presence of radiodense mineral in the newly formed bone nodules (white arrows) (100) **(f)** Enlargement of mineralized tissue formed adjacent to the nacre (note the lamellar structure). The spots analyzed by laser Raman spectroscopy (Fig. 4c, d) are at the center of the areas indicated by the open squares. **(g)** Photomicroradiograph of the mineralized tissue formed adjacent to the nacre. The lamellar structure of the newly mineralized matrix is again apparent (open triangles). Note the active bone cells with large nuclei and nucleoli (small black arrows) in close contact with the mineralized material (100). Samples in **(a), (d), (f)** and **(g)** were stained with basic fushin. Sample in **(b)** was stained with toluidine blue/methylene. Microradiographies (panels **c** and **e**) were performed as described in the method sections.

tals. In particular, peaks at 713 and 281 cm^{-1} which are typical of calcite were not observed.

Discussion

These studies demonstrate that nacre has strong osteogenic effects on human osteoblasts when placed in proximity to bone *in vitro*. The ability of nacre to stimulate osteogenesis *in vitro* should allow the clarification of the events involved in this process, and supports the idea that this material may be useful in clinical situations where the stimulation of osteogenesis is desirable. In addition, under the conditions of culture used, nacre can also promote the formation by osteoblasts of a structure with characteristics of nacre (lamellar organic matrix mineralized with aragonite). Given the unusual capacity of nacre in the presence of human osteoblasts *in vitro* to induce different types of mineralization, this model should provide insights in the specific interactions between matrix proteins and minerals which control the type of mineral produced in the course of biomineralization.

Bone Formation

When osteoblasts were cultured alone or in the presence of

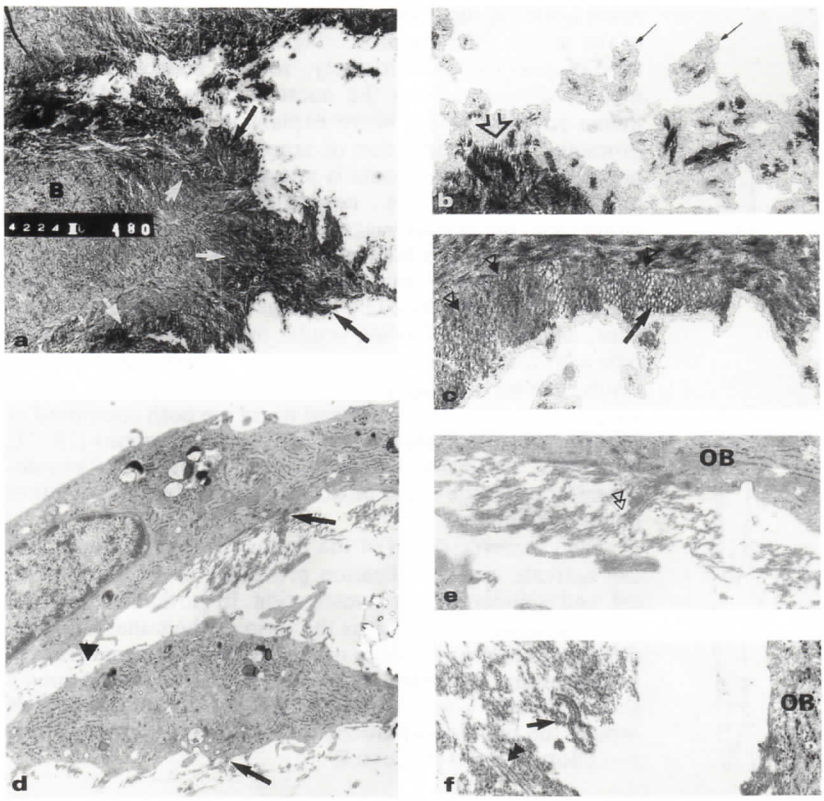

Fig. 3. Transmission electron micrographs of regions adjacent to the bone explant. **(a)** The interface between the bone explant and newly formed bone is indicated by the white arrow heads. Note that the newly formed tissue (woven bone) (black arrows) appears more electron dense than the adjacent bone explant (B) (3100). **(b)** High power view of the edge of newly formed bone showing needle-shaped apatite crystals (small black arrows) within matrix vesicles that have lost their membrane, and that are coalescent at sites adjacent to well-mineralized bone matrix (large unfilled arrow) (12,000). **(c)** Polygonal structures (black arrows) in close contact to newly formed bone. Note the interface between the two tissues (arrowheads) (12,000). **(d)** Active osteoblasts with cytoplasmic processes (black arrowheads), abundant rough endoplasmic reticulum, and intracytoplasmic vacuoles containing mineral. Note the extrusion of collagen fibrils (long black arrows) (8,500). **(e)** Higher magnification of the extrusion of collagen fibrils shown in panel d (arrowheads). OB = osteoblast (15,000). **(f)** Bone matrix formed by well cross-banded collagen fibrils (arrowheads) outside an osteoblast (OB). Some fibrils appear electrodense, due to mineralization (black arrow) (30,000).

bone fragments alone, no biomineralization occurred. Mineralization was demonstrated in previous studies, but in the presence of β-glycerophosphate [3–13]. These results underscore the difficulty in obtaining bone mineralization *in vitro*. In contrast, when nacre fragments were added to the cultures in proximity to bone, new bone formation occurred both by appositional growth on the existing bone and by the formation of mineralized nodules within the matrix adjacent to the bone explant. Electron microscopic evaluation of these sites demonstrated findings typical of those described in the course of bone formation *in vivo* [27, 28], and no evidence of toxicity was observed. Because bone formation depends on a series of complex events, a number of possible mechanisms could account for the ability of nacre to stimulate bone formation. It is noteworthy that a fibrous matrix did form when bone was placed adjacent to bone, but mineralization did not occur. Thus, studies evaluating the effects of nacre on the types of matrix proteins produced by human osteoblasts, the organization of the organic matrix, and the ion concentrations in the local milieu may give insights into the mechanisms responsible for the osteogenic properties of nacre.

"Nacre" Formation

The mineralized material forming in proximity to the nacre fragment was deposited as highly ordered lamellar sheets which were quite distinct from newly formed bone, but closely resembled the structure of nacreous shell. Thus, the determination of the chemical and structural nature of the crystals in this newly mineralized tissue was important. Laser Raman spectroscopy is the ideal microspectrometric crystal-chemical analytical technique for addressing this question. With the Raman "fingerprinting" technique used here, it is possible to obtain spectra of Raman-effect vibrations diffused from individual 1 μm^3 volumes of tissue without sample preparation and without sample alteration except for controllable local heating. Each different molecular or mineral species gives a different characteristic spectrum, and the identity (within experimental limits) of two spectra in terms of wavenumber positions of the peaks confirms the identity of the structures, and hence the chemical composition of the two samples. Thus, although the two polymorphs of $CaCO_3$, aragonite and calcite, give a prominent C-O vibration at around 1088 cm^{-1}, they can be distinguished by the 705 + 207 peaks of aragonite and the 713 + 281 peaks of calcite [24–26]. Amorphous $CaCO_3$, or any other phase, cannot create either of these sets of peaks which need the specific atomic arrangements existing only in aragonite and calcite, respectively. The laser Raman spectroscopic data that we obtained demonstrated that the newly mineralized tissue forming on the surface of the nacre fragment and in nodules of mineralized tissue formed adjacent to the nacre fragment was indeed aragonite (orthorhombic $CaCO_3$), not hydroxyapatite, calcite, amorphous $CaCO_3$, or any other mineral. It should be stressed that the laser Raman spectra obtained from newly mineralized tissue cannot be attributed to "contamination" from stray Raman diffusion from the nearby nacre explant for several reasons: (1) the position of the explant was not "near" on the micron scale (see Fig. 2f); (2) the analysis of unmineralized matrix adjacent to the mineralized nodules did not reveal any observable aragonite peaks, but did pick up stray Raman diffusion from the methylmethacrylate mounting medium; (3) the nacre explant could be dislodged from the newly mineralized material due to its greater rigidity and cleavage, and had been removed prior to evaluation of the samples. Thus, it is shown here for the first time that aragonite can, in fact, grow under the influence of living cells from mammals; and, given the lamel-

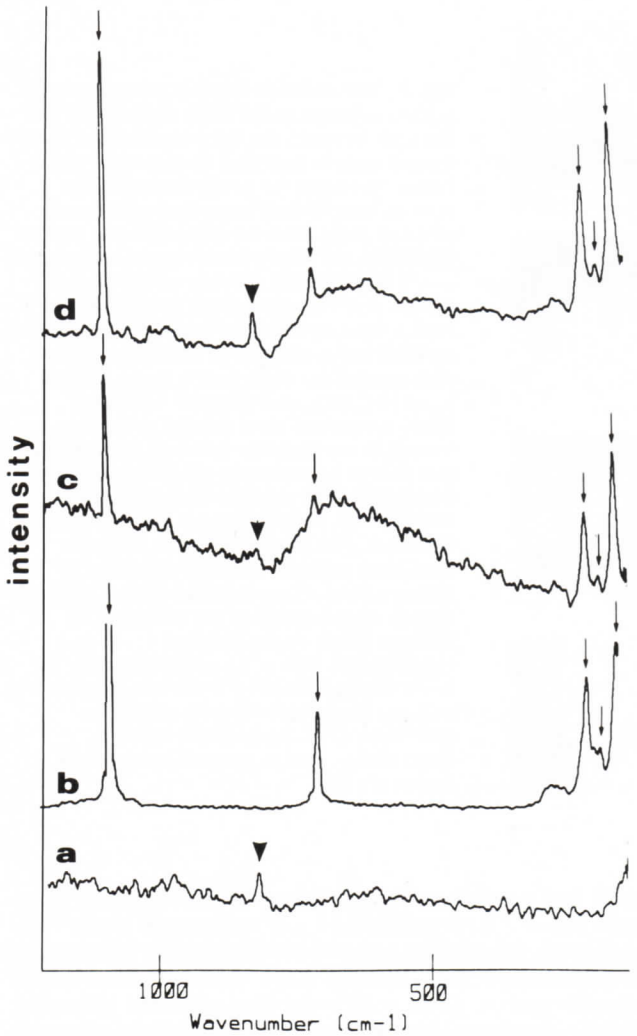

Fig. 4. Raman spectra determined on **(a)** the methylmethacrylate mounting medium as a blank; **(b)** a standard sample of nacre from which the explants were obtained; **(c)** the newly formed mineralized matrix forming on the surface of the nacre explant; **(d)** an isolated nodule of mineralized tissue formed within the matrix between the nacre and bone explants. The precise localization of tissues from which spectra c and d were obtained is shown in Figure 2f. The positive slope of the baseline between 690 and 790 cm^{-1} is artificial, and results from the joining of the two halves of the spectrum by weighted averaging. The spectra **c** and **d** both display all of the critical peaks (black arrows) for the characterization of orthorhombic $CaCO_3$ (aragonite) as determined by the standard spectrum **(b)** and in published spectra of aragonite [24–26]. Arrowheads indicate peak from the spectrum of methylmethacrylate.

lar texture, presumably due to organized layers of organic material, a nacre-like biomineral has been produced *in vitro*.

Biomineralization Process

The demonstration that osteoblasts, genetically programmed to make bone, could also promote the formation of a structure that had characteristics of nacre was unexpected. The specific geometry and charge of matrix proteins is thought to be an essential factor controlling the nucleation of a given mineral (e.g., the matrix is "epitactic") [20, 29]. In this context, it is possible that a biocrystalline structure such as nacre could, in turn, serve as a template for the organization of the matrix, thereby promoting the formation of the same type of material. Alternatively, soluble matrix proteins or mineral dissolved from the nacre may have modified the milieu adjacent to the nacre explant in such a way that it promoted the precipitation of aragonite. It is important to note that calcium carbonate is present in bone, but under an uncrystallized form (e.g., not aragonite or calcite) [30]. In either case, our results suggest that the constraints placed on mineral formation by human bone matrix proteins are not as specific as generally supposed. Both nacre and bone, mineralized tissues produced by phylogenetically distinct organisms, are formed following similar processes, in which specific cells (cells of the mantle for nacre, osteoblasts for bone) synthesize an organic matrix which is subsequently mineralized. The matrices of bone and nacre are both composed of fibrous proteins, proteoglycans, and acidic proteins [18, 31, 32]. Thus, these matrices may share fundamental physiochemical properties, and be able to substitute for each other in our system.

The characterization of the factors present in nacre that can activate biomineralization processes is obviously critical, and is under further investigation. In particular, it will be essential to determine if it is the form of the mineral (aragonite versus hydroxyapatite) or the demineralized matrix proteins that are important. Exploitation of this unique model should provide a new approach to the study of a variety of aspects of biomineralization, including the regulation and evolution of these processes.

Acknowledgments. We thank Allan Hance for a critical review of the manuscript, Michèle Garabédian for her strong support in these studies, Yves Deris, and Sophie Berland for their help in the iconography.

References

1. Raisz LG, Kream BE (1983) Regulation of bone formation. Part I. Med Prog 309:29–35, and Part II. Med Prog 309:83–89
2. Marks SC Jr, Popoff SN (1988) Bone cell biology: the regulation of development, structure, and function in the skeleton. Am J Anat 183:1–44
3. Tenenbaum HC, Heersche JNM (1982) Differentiation of osteoblasts and formation of mineralized bone in vitro. Calcif Tissue Int 34:76–79
4. Sudo H, Kodama HA, Amagai Y, Yamamoto S, Kasai S (1983) In vitro differentiation and calcification in a new clonal osteogenic cell line derived from newborn mouse calvaria. J Cell Biol 96:191–198
5. Robey PG, Termine JD (1985) Human bone cells in vitro. Calcif Tissue Int 37:453–460
6. Nefussi JR, Boy-Lefevre ML, Boulekbache H, Forest N (1985) Mineralization in vitro of matrix formed by osteoblasts isolated by collagenase digestion. Differentiation 29:160–168
7. Luria EA, Owen ME, Friedenstein AJ, Morris JF, Kuznetsow SA (1987) Bone formation in organ cultures of bone marrow. Cell Tissue Res 248:449–454
8. Ecarot-Charrier B, Shepard N, Charette G, Grynpas M, Glorieux FH (1988) Mineralization in osteoblast cultures: a light and electron microscopic study. Bone 9:147–154
9. Bhargava U, Bar-Lev M, Bellows CG, Aubin JE (1988) Ultrastructural analysis of bone nodules formed in vitro by isolated fetal rat calvaria cells. Bone 9:155–163
10. Benayahu D, Kletter Y, Zipori D, Wientroub S (1989) Bone marrow-derived stromal cell line expressing osteoblastic phenotype in vitro and osteogenic capacity in vivo. J Cell Physiol 140:1–7
11. Aronow MA, Gerstenfeld LC, Owen TA, Tassinari MS, Stein GS, Lian LB (1990) Factors that promote progressive develop-

ment of the osteoblast phenotype in cultured fetal rat calvaria cells. J Cell Physiol 143:213–221
12. Gotoh Y, Hiraiwa K, Nagayama M (1990) In vitro mineralization of osteoblastic cells derived from human bone. Bone Miner 8:239–250
13. Kasugai S, Todescan Jr R, Nagata T, Yao KL, Butler WT, Sodek J (1991) Expression of bone matrix proteins associated with mineralized tissue formation by adult rat bone marrow cells in vitro: inductive effects of dexamethasone on the osteoblastic phenotype. J Cell Physiol 147:111–120
14. Khouja HI, Bevington A, Kemp GJ, Russel RGG (1990) Calcium and orthophosphate deposits in vitro do not imply osteoblast-mediated mineralization: mineralization by β-glycerol phosphate in the absence of osteoblasts. Bone 11:385–391
15. Gronowicz G, Woodiel FN, McCarthy MB, Raisz LG (1989) In vitro mineralization of fetal rat parietal bones in defined serum-free medium: effect of β-glycerol phosphate. J Bone Miner Res 4:313–324
16. Camprasse S, Camprasse G, Pouzol M, Lopez E (1990) Artificial dental root made of natural calcium carbonate (bioracine). Clin Mater 5:235–250
17. Silve C, Grosse B, Tau C, Garabédian M, Fritsch J, Delmas PD, Cournot-Witmer G, Balsan S (1986) Response to parathyroid hormone and 1,25-dihydroxyvitamin D_3 of bone-derived cells isolated from normal children and children with abnormalities in skeletal development. J Clin Endocrinol Metab 62:583–590
18. Taylor JD, Kennedy WJ, Hall A (1969) The shell structure and mineralogy of the bivalvia. Bulletin of the British Museum (Natural History) (suppl 3) Zoologie
19. Bevelander G, Nakahara H (1969) An electron microscope study of the formation of the nacreous layer in the shell of certain bivalve molluses. Calcif Tissue Res 3:84–92
20. Simkiss K, Wilbur KM (1989) Biomineralization. Academic Press Inc, Harcourt Brace Jovanovitch Publishers, San Diego, London, p 337
21. Lopez E, Peignoux-Deville J, Lallier F, Martelly E, Milet C (1976) Effects of calcitonin and ultimobranchialectomy (UBX) on calcium and bone metabolism in the eel, *Anguilla anguilla* L. Calcif Tissue Res 20:173–186
22. Lopez E, Baud CA, Boivin G, Lallier F (1978) Etude ultrastructurale chez un poisson téléostéen, l'anguille *Anguilla anguilla* L., des processus de mineralisation dans les cas d'une ossification périchondrale de l'arc branchial et d'une apposition secondaire dans l'os vertebral. Ann Biol Anim Bioch Biophys 18(1): 105–117
23. Delhaye M, Dhamelincourt P (1975) Raman microprobe and microscope with laser excitation. J Raman Spectroscopy 3:33–43
24. Smith DC (1987) Raman spectroscopy of natural and synthetic minerals: a review. Terra Cognita 7:20–21
25. Pinet M, Smith DC, Lasnier B (in press) Utilité de la spectrométrie Raman pour l'identification des gemmes, et compilation de leurs spectres Raman. Bull Asso Franç Gemmol
26. Vénec-Peyré MT, Jaeschke-Boyer H (1978) Application de la microsonde moléculaire à laser Mole à l'étude du test de quelques Foraminifères calcaires. C R Acad Sc Paris 287, série D:607–609
27. Glimcher MJ (1984) Recent studies of the mineral phase in bone and its possible linkage to the organic matrix by protein-bound phosphate bonds. Phil Trans R Soc Lond 304:479–507
28. Landis WJ (1985) Temporal sequence of mineralization in calcifying turkey leg tendon. In Butler WT (ed) The chemistry and biology of mineralized tissues. Ebsco Media, Inc. Birmingham, Alabama, pp 360–363
29. Weiner S, Addadi L (1991) Acidic macromolecules of mineralized tissues: the controllers of crystal formation. TIBS 16:252–256
30. Woodward HQ (1964) The composition of human cortical bone. Clin Orthop 37:187–193
31. Wheeler AP, George JW, Evans CA (1981) Control of calcium carbonate nucleation and crystal growth by soluble matrix of oyster shell. Science 212:1397–1398
32. Mann S (1988) Molecular recognition in biomineralization. Nature 332:119–124

Substitution de la racine dentaire par des squelettes d'invertébrés aquatiques chez l'animal et l'homme

PAR

Georges CAMPRASSE, Serge CAMPRASSE
et Gabriel A. GILL

Extrait des *Comptes rendus de l'Académie des Sciences*
30 août 1988

Médecine et thérapeutique/*Medicine and Therapeutics*

Substitution de la racine dentaire par des squelettes d'invertébrés aquatiques chez l'animal et l'homme

Georges CAMPRASSE, Serge CAMPRASSE et Gabriel A. GILL

Résumé — La biocompatibilité entre l'os des mammifères, l'aragonite et la calcite sécrétées par les invertébrés aquatiques (Coraux, Mollusques) nous a conduits, après expérimentation animale, à implanter chez les humains des racines dentaires artificielles en $CaCO_3$ qui, incorporées mais non résorbées, supportent une restauration prothétique. Un dispositif assure l'étanchéité entre la racine artificielle et le milieu buccal, ainsi que l'amortissement des chocs. Désormais, cette nouvelle possibilité d'implantation des racines artificielles d'excellent comportement entraînera des modifications certaines dans la pratique des soins dentaires.

Substitution of dental roots by aquatic invertebrate skeletons in animals and humans

Abstract — *The biocompatibility of mammal bone with aragonite and calcite skeletons of aquatic invertebrates (Corals, Molluscs) led us, after animal experimentation, to implant in humans artificial dental roots derived from such invertebrates. These roots, incorporated but not resorbed, serve as supports for a prosthetic crown; they are equipped to isolate the root from the buccal cavity and to ensure shock absorbtion during mastication. The greater ease of implanting artificial teeth and their excellent acceptance will in many cases modify the strategy of current dental treatment.*

Abridged English Version — INTRODUCTION. — The compatibility of porous calcium carbonate coral skeletons with mammal bone has been the subject of study, mainly in orthopaedy and cranio-facial surgery ([1] to [5]). In all cases the aim was the rapid transformation of the coral into newly formed bone. The excellent acceptance of these materials has led us to experiment the substitution of dental roots by invertebrate skeletons of corals and bivalves, first in dogs and then in humans.

METHODS. — We chose hard compact calcium carbonate of limited porosity to prevent the penetration of osteons and the consequent transformation of the grafted material into neoformed bone. For these reasons, the octocoral *Corallium johnsoni* Gray and the bivalve *Pinctada margaritifera* (L.) were used. These materials are turned into cylindrical screws of various dimensions to serve as dental roots (*Fig.* 14*a*). Their tight insertion allows immediate adherence, followed by a rapid osteo-integration.

Pre-surgery study of scannograph projections is made to determine orientation, quality and quantity of bone in the locality to be implanted.

The artificial roots are equipped with a superstructure that provides support for a prosthetic crown and offers two innovations: it favours an epithelial attachment comparable to that of the natural tooth (*Fig.* 14*a*) and substitutes the alveolo-dental ligament in absorbing stresses and shocks due to mastication (*Fig.* 14*b*). Current surgical protocols of oral implantology have been followed, using a low speed drill (1,200 revs/min.), yet with an internal flow of cooling physiological serum at 0°C, which is also used to keep the artificial root cold until insertion.

RESULTS AND DISCUSSION. — There is perfect compatibility of the introduced material with the bone and excellent and rapid osteointegration, undoubtedly due to physico-chemical

Note présentée par Yves COPPENS.

0249-6313/88/03070485 $2.00

affinities between the $CaCO_3$ composing the artificial roots (aragonite or calcite) and the $CaPO_4$ of the bone (*Figs.* 1-13 *a*, *b*; 15 *d*).

The application of low temperature during surgery is new and brings distinct improvements in the post-surgical reaction. These are a diminution of bleeding, of extravasation and subsequent oedema, of ischaemia due to anaesthesis and a reduction in pain.

After many months of use, no modification in outline of the grafted roots has been noted. This confirms our hypothesis that the poor porosity does not allow the osteoclasts to penetrate and disintegrate the material nor the osteoblasts to produce new bone tissue.

Of over one hundred inserted roots, eight had to be extracted. Six had previously developed apical lesions and two at the chin symphysis, due to faulty drill orientation. Six were replaced successfully.

Because of the relative simplicity of these techniques and the quality of the outcome, they should find ready acceptance in current dental practice.

AVANT-PROPOS ET OBJECTIFS. — Le squelette du corail, vu sa ressemblance avec le tissu osseux, a inspiré récemment plusieurs démarches de restauration thérapeutique : *a*, l'utilisation du corail comme modèle d'implant en hydroxyapatite (HAP) — chimiquement et structuralement proche de l'os ([6], [7], [8]); *b*, la confection de prothèses poreuses et rugueuses (« madréporiques »), favorisant un ancrage par ostéogenèse [9]; *c*, l'implantation directe de corail se pratique surtout en France en chirurgie orthopédique et réparatrice ([1] à [5]), avec comblement par résorption totale du corail et développement simultané d'un os néoformé; *d*, l'utilisation de poudre de corail comme matériau de comblement en chirurgie osseuse.

Il est actuellement proposé, pour remplacer les racines dentaires, des implants en titane et en céramique, matériaux de nature très éloignée de celle du tissu osseux. Vu la compatibilité entre l'os en $CaPO_4$ et le $CaCO_3$ du squelette de nombreux invertébrés aquatiques, il nous est apparu qu'un implant en $CaCO_3$ dur, dont la compacité empêcherait la pénétration de la cellule osseuse, constituerait une racine dentaire artificielle inaltérable.

Au préalable voici un rappel anatomique de la dent naturelle. Enchassée dans une alvéole et fixée par le ligament alvéolo-dentaire, la racine est surmontée d'une couronne. A l'émergence de celle-ci dans la cavité buccale, la gencive adhère par « l'attache épithéliale ». Une sertissure étanche isole ainsi les tissus sous-jacents du milieu buccal.

C'est pourquoi nous avons conçu une supra-structure aux dimensions des racines artificielles qui permet une adhésion de la gencive réalisant une véritable « attache épithéliale artificielle » (*fig.* 14 *a*). Ce même dispositif, comme le ligament, amortit pressions et chocs masticatoires.

Les racines artificielles, une fois l'ostéo-intégration réalisée, reçoivent un support de prothèse (*fig.* 14 *b*).

PROCÉDÉ ET RÉSULTATS CLINIQUES. — *Carbonate utilisé.* — D'après la littérature, les coraux suivants ont été implantés et bien tolérés en chirurgie : *a*, Scléractiniaires : *Porites, Synaraea, Acropora, Fungia, Favites, Acanthastraea, Turbinaria; b*, Hydrozoaires : *Millepora, Steganopora.* Toutefois leur bonne détermination ne semble pas toujours garantie.

Les Scléractiniaires ont une microstructure essentiellement en faisceaux de fibres, disposés autour d'un axe pour former les trabécules, éléments majoritaires du squelette. Les Millepores et les Stylasters sont également trabéculaires.

Les squelettes des formes mentionnées sont en aragonite, minéral métastable de $CaCO_3$. La compatibilité des squelettes aragonitiques avec l'os est donc acquise.

Parmi les formes à squelette solide et compact, nous avons retenu :

1. *Herpolitha*, *Fungia*, *Halomitra*, *Polyphyllia* (Scleractinia, Fungiidae), chez qui la bande basale est renforcée par : *a*, les directions plutôt croisées des trabécules à croissance vers le haut et vers le bas, *b*, le trajet des fultures indépendant de celui des trabécules, *c*, la soudure des fultures à deux cloisons voisines, *d*, la cimentation stéréoplasmique [10].

2. *Corallium johnsoni* Gray (Octocorallia, Gorgonacea). Ici l'axe est en calcite, de structure composite et multidirectionnelle. Une phase fibreuse en faisceaux est suivie d'une sécrétion de monocristaux cylindriques bordés de lamelles, ce qui donne à l'axe de *C. johnsoni* une compacité et une solidité élevées [11]. La parfaite intégration du polypier comme implant témoigne de l'acceptation de la calcite par l'os.

3. *Pinctada margaritifera* (L.) (Mollusca, Bivalvia), à coquille calcitique et aragonitique. La couche nacrée, en aragonite, est compacte et très résistante, sans doute grâce aux soudures particulières de ses plaquettes ([12], [13]).

Les racines artificielles, cylindriques, à filetage particulier, sont fournies et stérilisées par Biocorex Industries, France (*fig.* 14 *a*, *b*).

Description des opérations. — Les racines artificielles ont été insérées aux maxillaires supérieur et inférieur : *a*, immédiatement après extraction, dans les alvéoles naturelles, par mise en conformité de celles-ci (forage et taraudage), enfouissement de la racine et suture hermétique; *b*, dans les cas d'édentations, dans des alvéoles artificielles après mise à nu de l'os, forage et taraudage.

Le forage (1 200 tr/mn) et le taraudage se font sous refroidissement interne de sérum physiologique réfrigéré. La racine artificielle est maintenue jusqu'à son insertion dans du sérum physiologique à 0°C. Ce procédé original présente des avantages incontestables par la diminution : *a*, du saignement, *b*, de l'extravasation avec pour conséquence une absence d'œdème, *c*, de l'ischémie par l'anesthésie, *d*, du phénomène inflammatoire et, partant, diminution considérable de réaction douloureuse.

Patients	Age	Zones implantées	Dates	Diamètre des racines (mm)	Planche	Remarques
M. J. C. L.	43	33/43 et 22	12.85	5	*fig.* 1	
M^{me} C. S.	42	14	12.85	5	*fig.* 2	Extraction
M. R. G.	52	35 et 45	12.85	5 et 6	*fig.* 3	Extraction de 34 et 44
M. C. P.	27	12	12.85	5	*fig.* 4	Extraction
M^{me} W. L.	37	13 à 16, 23 à 26	1.86	5 et 6 (4 racines)	*fig.* 5	Edentation
M^{me} P. M. C. . . .	42	26	11.85	10	*fig.* 6	Après extraction
M^{me} S. D.	29	23-24	1.86	6 (2 racines)	*fig.* 7	Agénésie
M^{me} C.	42	46	1.86	8 et 10 (2 racines)	*fig.* 8	Extraction de 47
M^{me} A. L.	36	15 et 25	3.86	6	*fig.* 9	
M^{me} T.	52	15	3.86	5	*fig.* 10, 13 *a*, *b*	
M^{me} L. S.	27	45	1.86	7 (2 racines)	*fig.* 11	Extraction de 46
M. R. J. L.	50	22 à 25	4.86	5 et 6 (3 racines)	*fig.* 12	Edentation

Cas cliniques. — Le choix a porté sur des cas d'édentations, d'agénésie et d'extractions. Outre des examens biologiques et fonctionnels (NF/S, glycémie, T.S., T.C., T.C.K., E.C.G.), il a été pratiqué des examens scannographiques avec notamment des incidences occlusales. Des coupes jointives de 2 mm, permettent une évaluation qualitative et quantitative des sites à implanter.

Les figures 13 *a* et 13 *b* montrent l'aspect radiologique de la réalisation prothétique au niveau de 15.

Parmi les nombreux cas traités, sont cités ici ceux qui présentent le plus grand recul dans le temps. Tous manifestent une parfaite tolérance du matériau implanté, une ostéo-intégration rapide, vraisemblablement générée par une ostéo-induction déclenchée par chimiotactisme.

D'autre part, notre hypothèse se confirme : la faible porosité du matériau ne permet pas la pénétration des ostéoclastes et, partant, sa transformation en tissu osseux par les ostéoblastes. Les racines artificielles ne semblent subir aucune altération dans le temps.

Sur plus de cent racines insérées, huit ont dû être ôtées; six insérées après extraction de dents ayant développé des lésions apicales, deux à la symphyse mentonnière, mal orientées au forage. Six ont pu être replacées avec succès.

DISCUSSION ET CONCLUSIONS. — Notre but était de démontrer la parfaite biocompatibilité entre l'os maxillaire et le $CaCO_3$ naturel des squelettes d'invertébrés aquatiques (Madréporaires, Mollusques). L'étude a porté entre autres sur *Corallium johnsoni* et *Pinctada* aux propriétés mécaniques et physiques les plus aptes à la réalisation de racines artificielles. Or, les examens cliniques et radiologiques ont prouvé qu'au bout de 3 ans, les racines artificielles en $CaCO_3$ très dur et compact ne montrent aucune modification de forme ni de structure.

Il apparaît désormais possible d'utiliser, en implantologie orale et en pratique courante, des racines artificielles en $CaCO_3$ naturel (Madréporaires, Mollusques, etc.). Le protocole opératoire, simple, obéit aux exigences de la chirurgie orale. La possibilité d'insérer des racines artificielles immédiatement après extraction amènera une modification importante du comportement de l'omnipraticien.

On peut noter les innovations permettant une adhésion histologique de la muqueuse autour de la racine et l'absorption des chocs.

Les résultats de ce travail confirment la parfaite biocompatibilité tant de l'aragonite que de la calcite.

La biocompatibilité accrue est due à l'origine naturelle du matériau et très probablement à la similitude physico-chimique entre le $CaCO_3$ et le $CaPO_4$ du tissu osseux, comme il ressort de l'aspect radiologique.

L'ostéo-intégration rapide semble être générée par une ostéo-induction due à un chimiotactisme du matériau sur la cellule osseuse.

Soulignons les avantages per- et post-opératoires d'une nouvelle technique de refroidissement qui consiste en : — la réfrigération du sérum physiologique (0°C) utilisé pour le refroidissement interne des instruments rotatifs; — le maintien de la racine artificielle dans le sérum physiologique réfrigéré à 0°C jusqu'à son insertion.

Nous remercions sincèrement le Service de Recherche du Laboratoire Lucien (28 Luisant), MM. G. Schnedecker et A. Le Margne (D.P.C., Saclay), P. Luong (Laboratoire de Mécanique des Solides, École Polytechnique, Palaiseau), M^mes^ E. Lopez, F. Lalier, S. Freneix, S. Barta-Calmus, MM. P. Clément, M. Lemoine, D. E. Russel (M.N.H.N. Paris), M^mes^ C. Privé-Gill (Univ. Paris-VI), M. Rzond (Chelles) et C. Pringet (Biocorex, Aubervilliers), Prof. W. R. Stern (U.W.A., Perth, Australie), M. J. Mazet (46 Gourdon).

Note reçue le 1^er^ juillet 1988, acceptée le 18 juillet 1988.

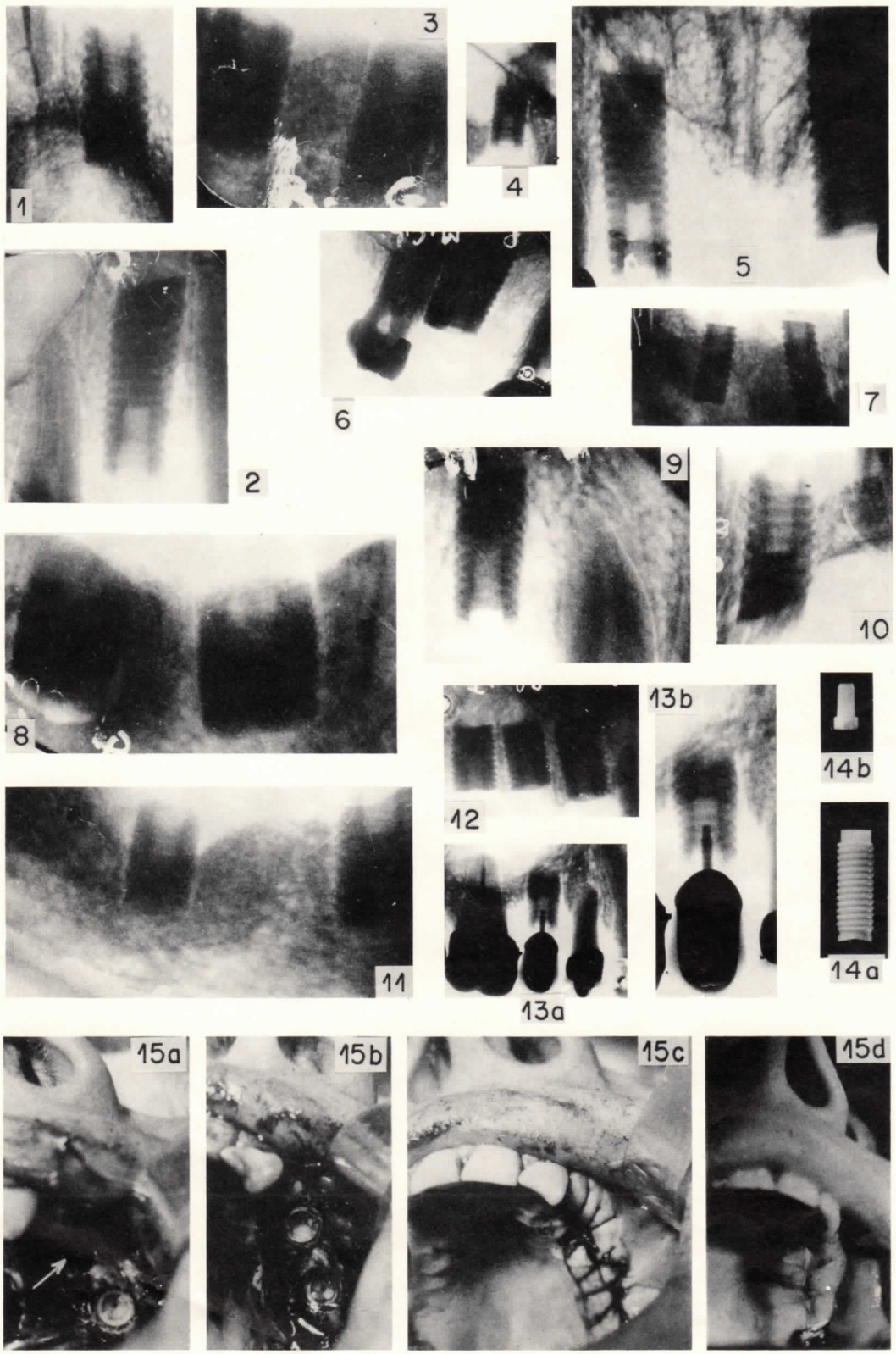
1
3
4
5
2
6
7
9
10
8
12
13b
14b
11
14a
13a
15a
15b
15c
15d

RÉFÉRENCES BIBLIOGRAPHIQUES

[1] A. F. PATEL, G. HONNART, G. GUILLEMIN et J.-L. PATAT, *Chirurgie*, 106, 1980, p. 199-205.

[2] G. GUILLEMIN, J. FOURNIE, J.-L. PATAT et M. CHETAIL, *C. R. Acad. Sci. Paris*, 293, série III, 1981, p. 371-376.

[3] Y. LEVET et G. YOST, *Ann. Chir. Plast. Esthét.*, 18, 1983, p. 180-181.

[4] F. SOUYRIS, J.-P. CHEVALIER, C. PAYROT, C. PELLEQUER, A. GARY-BOBO et C. MERLIER, *Ann. Chir. Plast. Esthét.*, 29, n° 3, 1984, p. 256-260.

[5] C. SERVERA, F. SOUYRIS, C. PAYROT et P. JAMMET, *Rev. Stomatol. Chir. Maxillofac.*, 88, n° 5, 1987, p. 326-333.

[6] D. M. ROY et S. K. LINNEHAM, *Nature*, 247, n° 5438, 1974, p. 220-222.

[7] R. T. CHIROFF, R. A. WHITE, E. N. WHITE, J. N. WERBERT et D. M. ROY, *J. Biomed. Mat. Res.*, 11, 1977, p. 165-178.

[8] R. E. HOLMES, *Plast. Reconst. Surg.*, 63, 1979, p. 626-633.

[9] G. LORD, J.-H. MAROTTE, J.-P. BLANCHARD, J.-L. GUILLAMON et M. GORY, *Rev. Chir. Orthop.*, supp. II, 64, 1978, p. 5-13.

[10] G. A. GILL, *Acta Pal. Pol.*, 25, (3-4), 1980, p. 301-310.

[11] A. LAWNICZAK, *Senckenbergiana Marit.*, 19, (3-4), 1987, p. 149-161.

[12] K. WADA, *J. Electronmicros.*, 9, n° 1, 1960, p. 21-23.

[13] J. D. TAYLOR, W. J. KENNEDY et A. HALL, *Bull. Brit. Mus. (Nat. Hist.) Zool.*, 3, 1969, p. 1-125.

G. C. et S. C. : 63, *avenue de la Résistance*, 77500 *Chelles ;*

G. A. G. : *C.N.R.S., Muséum national d'Histoire naturelle, Institut de Paléontologie*, 8, *rue de Buffon*, 75005 *Paris.*

EXPLICATIONS DE LA PLANCHE

Fig. 1-13. – Aspects radiologiques des cas cliniques.

Fig. 1-13. – *X-ray photos of clinical cases.*

C. j. = *Corallium johnsoni* Gray; P.m. = *Pinctada margaritifera* (L.)

Fig. 1. – (J.C.L.) Radio de 22. Saillie de la racine artificielle dans le sinus maxillaire (cliché 7 mois après l'intervention) (C.j.) (G × 2).

Fig. 1. – (*J.C.L.*) *X-ray photo at* 22. *Insertion of an artificial root with slight penetration into the maxillary sinus* (*photographed* 7 *months after surgery*) (*C.j.*) (*M* × 2).

Fig. 2. – (C.S.) Radio de 14. Parfaite ostéo-intégration (6 mois après l'intervention) (C.j.) (G × 3).

Fig. 2. – (*C.S.*) *X-ray photo at level* 14. *Perfect integration of the artificial root* (6 *months after surgery*) (*C.j.*) (*M* × 3).

Fig. 3. – (R.G.) Radio de 34/35. Liaison intime entre les racines artificielles et l'os maxillaire (après 7 mois) (C.j.) (G × 2).

Fig. 3. – (*R.G.*) *X-ray photo at level* 34/35. *Note the incorporation of the artificial roots in the maxillary bone* (*after* 7 *months*) (*C.j.*) (*M* × 2).

Fig. 4. – (C.P.) Pénétration de l'extrémité de la racine (niveau 12) dans le sinus maxillaire (après 7 mois) (C.j.) (G × 1).

Fig. 4. – (*C.P.*) *Penetration of the root end* (*level* 12) *into the maxillary sinus showing perfect acceptance* (*after* 7 *months*) (*C.j.*) (*M* × 1).

Fig. 5. – (W.L.) Racines artificielles à 23 et 25. Vascularisation importante et ostéo-intégration (après 23 mois) (C.j.) (G × 2).

Fig. 5. – (*W.L.*) *Artificial roots at levels* 23 *and* 25. *Active vascularization with osteo-integration* (*after* 23 *months*) (*C.j.*) (*M* × 2).

Fig. 6. – (P.M.C.) Remplacement de 26 par une racine de 10 mm ∅ (après 8 mois) (C.j.) (G × 1).

Fig. 6. – (*P.M.C.*) *Substitution of tooth* 26 *by a root of* 10 *mm diameter* (*after* 8 *months*) (*C.j.*) (*M* × 1).

Fig. 7. – (S.D.) Remplacement de 23 et 25, parfaite biocompatibilité (après 6 mois) (P.m.) (G × 1).

Fig. 7. – (*S.D.*) *Substitution of* 23 *and* 25; *perfect biocompatibility* (6 *months after surgery*) (*P.m.*) (*M* × 1).

Fig. 8. – (C.) Racines artificielles de 8 et 10 mm ∅ aux niveaux 46 et 47 (après 6 mois) (P.m.) (G × 2).

Fig. 8. – (*C.*) *Artificial roots of* 8 *and* 10 *mm diameter at levels* 46 *and* 47 (*after* 6 *months*) (*P.m.*) (*M* × 2).

Fig. 9. – (A.L.) Racine artificielle à 15 (après 6 mois) (P.m.) (G × 2).

Fig. 9. – (*A.L.*) *Artificial root at level* 15 (*after* 6 *months*) (*P.m.*) (*M* × 2).

Fig. 10. – (T.) Racine artificielle à 15; irruption au plancher du sinus maxillaire; excellente intégration (après 6 mois) (C.j.) (G × 2).

Fig. 10. – (*T.*) *Artificial root at* 15 *with introduction into the floor of the maxillary sinus; perfect acceptance* (*after* 6 *months*) (*C.j.*) (*M* × 2).

Fig. 11. – (L.) Racines artificielles à 45 et 46. Matérialisation du canal dentaire (après 7 mois) (P.m.) (G × 2).

Fig. 11. – (*L.*) *Artificial roots at* 45 *and* 46. *Note the presence of the dental canal* (*after* 7 *months*) (*P.m.*) (*M* × 2).

Fig. 12. – (R.J.L.) Excellente vascularisation entre trois racines artificielles à 22, 23 et 25 (après 6 mois) (P.m.) (G × 1).

Fig. 12. – (*R.J.L.*) *Excellent vascularization between three artificial roots at* 22, 23 *and* 25 (*after* 6 *months*) (*P.m.*) (*M* × 1).

Fig. 13 *a*, *b*. – Aspect radiologique de la racine artificielle (15) surmontée de sa suprastructure (non radioopaque), sa vis en titane et la prothèse en céramique (après 12 mois). *a* (G × 1); *b* (G × 2).

Fig. 13 *a*, *b*. – *X-ray image of the artificial root* (15) *and its superstructure* (*not opaque to X-rays*), *its titanium screw and the ceramic crown* (*after* 12 *months*). *a* (*M* × 1); *b* (*M* × 2).

Fig. 14 *a*, *b*. – Racine artificielle avec sa suprastructure (14 *a*) et son support de prothèse (14 *b*) (Biocorex Industries) (G × 1).

Fig. 14 *a*, *b*. – *Artificial root with its superstructure* (14 *a*) *and its prosthetic support* (14 *b*) *supplied by Biocorex Industries* (*M* × 1).

Fig. 15 *a*, *b*, *c*, *d*. – Insertion de deux racines artificielles (S.D., *fig.* 7). *a*, alvéole artificielle (flèche) à 23 et racines à 25; la partie visible est la suprastructure; *b*, les deux racines en place; *c*, la muqueuse après suture hermétique; *d*, ablation des fils et cicatrisation après 5 jours.

Fig. 15 *a*, *b*, *c*, *d*. – *Fixing of two artificial roots* (*clinical case S.D.*, Fig. 7). *a, note the drilled hole* (*arrow*) *at* 23 *and the artificial root at* 25 *with its superstructure is visible; b, both roots in place; c, the gum hermetically sutured; d, healing after* 5 *days, sutures removed.*